A Numerical Study on MHD 3-D Casson-Nanofluid Flow Past an Exponentially Stretching Sheet with Double Cattaneo-Christov Diffusion Effects

Murali Gundagani[1,*], Venkata Madhu Javvaji[2], Deepa Gadipalli[3], Suresh Pallerla[3], Qasem M. Al-Mdallal[4] and S. M. Bhati[5]

[1] Department of Freshman Engineering, Geethanjali College of Engineering and Technology, Cheeryal, Hyderabad, 501301, India

[2] Department of Mathematics, Sreenidhi Institute of Science and Technology, Yamnampet, Hyderabad, 501301, India

[3] Department of Mathematics, Chaitanya Bharathi Institute of Technology, Gandipet, Hyderabad, 500075, India

[4] Department of Mathematical Sciences, United Arab Emirates University, Abu Dhabi, P.O. Box 15551, United Arab Emirates

[5] Department of Engineering Science, KBT College of Engineering, Nashik, 422013, India

INFORMATION

Keywords:
Three dimensional
exponentially stretching sheet
casson fluid
magnetic field
nanofluid
cattaneo-christov double diffusion
runge kutta method
shooting technique

DOI: 10.23967/j.rimni.2025.10.63195

SCIPEDIA Revista Internacional de Métodos Numéricos para Cálculo y Diseño en Ingeniería

Revista Internacional Métodos numéricos para cálculo y diseño en ingeniería RIMNI CIMNE

A Numerical Study on MHD 3-D Casson-Nanofluid Flow Past an Exponentially Stretching Sheet with Double Cattaneo-Christov Diffusion Effects

Murali Gundagani[1,*], Venkata Madhu Javvaji[2], Deepa Gadipalli[3], Suresh Pallerla[3], Qasem M. Al-Mdallal[4] and S. M. Bhati[5]

[1]Department of Freshman Engineering, Geethanjali College of Engineering and Technology, Cheeryal, Hyderabad, 501301, India

[2]Department of Mathematics, Sreenidhi Institute of Science and Technology, Yamnampet, Hyderabad, 501301, India

[3]Department of Mathematics, Chaitanya Bharathi Institute of Technology, Gandipet, Hyderabad, 500075, India

[4]Department of Mathematical Sciences, United Arab Emirates University, Abu Dhabi, P.O. Box 15551, United Arab Emirates

[5]Department of Engineering Science, KBT College of Engineering, Nashik, 422013, India

ABSTRACT

A numerical study of a three-dimensional steady-state flow of a viscous incompressible Casson fluid containing nanofluid particles interacting with a stretching sheet is the primary focus of this work. The equations for concentration and energy include the Cattaneo-Christov double diffusion effects. This work transforms deriving the controlling boundary layer equations into similarity equations using non-linear similarity transformations in three-dimensional analyses. To evaluate this study, the following was done. In the case of the combined Runge-Kutta method and the shooting approach, it is possible to provide an analytical solution for the obtained equations. Moreover, a comparative analysis of the collected data with previously published results under certain circumstances demonstrates a significant concordance between the two sets of findings. The problem is governed by thirteen physical parameters. Figures and tables are used to depict the effects of different characteristics in the following chapters, including temperature, velocity, and concentration profiles, on distinct flow distributions.

OPEN ACCESS

Received: 08/01/2025

Accepted: 28/03/2025

Published: 20/04/2025

DOI
10.23967/j.rimni.2025.10.63195

Keywords:
Three dimensional
exponentially stretching sheet
casson fluid
magnetic field
nanofluid
cattaneo-christov double diffusion
runge kutta method
shooting technique

1 Introduction

Stretching-induced flows play an important part in industrial manufacturing, influencing the production of polymers and rubber and also in the annealing and thinning of copper wire, spinning

*Correspondence: Murali Gundagani (uraligundagani@gmail.com).

fiber cooling, and extrusion from dye or polymer filaments. These flows are not just mechanical phenomena but are integral to the desired properties and performance characteristics of the materials. Furthermore, the application of fluid dynamics extends beyond these processes, as evidenced by the operation of heat exchangers, the technique of crop freezing, the design of air conditioning systems, the efficiency of solar power collectors, the functionality of cooling towers, and the innovation in desalination technologies.

Because of its applications in engineering and industrial processes, the study of magnetohydrodynamic (MHD) fluxes and heat transfer in complicated fluid systems has attracted a lot of interest. Using magnetohydrodynamics, Nadeem et al. [1] investigated boundary layer flow over a bi-directional stretched sheet and came up with a series solution. While Akbar et al. [2] examined the impact of MHD on nanofluid flow with double diffusion across a stretched surface, Sadiq et al. [3] examined the characteristics of unsteady nanofluid flow on a stretching sheet with convective boundary conditions. Ali et al. [4] investigated heat and mass transfer on porous expanding and contracting surfaces, whereas Hussain et al. [5] investigated the nanofluid flow sensitivity across extended surfaces. Analytical and computational techniques were used in these and other research [6–10] to comprehend fluid dynamics across stretched sheets. Heat conduction law is often used to explain heat transfer, a basic process. Nevertheless, there are drawbacks to Fourier's law, such as its inability to consider immediate temperature fluctuations. The Cattaneo-Christov heat flux model, which depicts heat transmission as thermal waves traveling at limited speeds, was created as a result of Cattaneo's [11] introduction of thermal relaxation into Fourier's law. Numerous research has made extensive use of this concept. For example, Mustafa [12] used it to Maxwell fluid flow, while Ciarletta et al. [13] utilized it to investigate system stability. Its implications in Newtonian and viscoelastic fluids were subsequently investigated by Straughan [14] and Han et al. [15], respectively. These investigations demonstrate how crucial the Cattaneo-Christov model is to comprehending heat transmission in complex fluid systems. Because of their industrial significance, non-Newtonian fluids like Casson and nanofluids have also been the subject of much research. Babu et al. [16] examined Casson fluid flow in porous media with heat transfer and Hall currents, While Deepa and Murali [17] examined unsteady MHD flow with thermophoresis and viscous dissipation, whereas Kirubaharan et al. [18] investigated double diffusion effects in Casson-nanofluid flow. Gundagani et al. [19,20] investigated nanofluid flow under MHD and convective boundary conditions. Furthermore, Murali et al. [21,22] studied thermophoresis and Brownian motion in nanofluids, and references [23–25] had a lot of impact on the present reported work. Cited references [26–28] model analyzed heat and mass transfer effects and showed the practical uses of their study. These investigations highlight how chemical reactions, magnetic fields, and porous media may improve heat and mass transport. Research has been focused on the impact of radiation on MHD flows and heat transfer in porous media. Magneto hydrodynamic applications were shown in their studies [29,30] and improved knowledge of radiation. Madan Kumar et al. [31] investigated Jeffrey fluid flow with activation energy, whereas Venkatesh et al. [32] investigated MHD Maxwell nanofluid flow with heat radiation. Rajakumar et al. [33] examined MHD convection with radiation absorption and Hall currents, whereas Suhasini et al. [34] examined micropolar nanofluid flow with Brownian motion and thermophoresis. Carreau nanofluid flow with radiative heat sources was examined by Mebarek-Oudina et al. [35], with a focus on applications in medical engineering and renewable energy. The area has been further broadened by recent research. Anantha Kumar et al. [36,37] studied Casson fluids with heat radiation and changing viscosity effects, whereas Rathore et al. [38] assessed MXene-based nanofluids on curved surfaces. Elattar et al. [39] and Khan et al. [40] highlighted applications in thermal systems and environmental engineering while concentrating on irregular heat sources and waste discharge in Eyring-Powell nanofluids. In their study [41–44] on Mathematical Modelling of

Fluid Dynamics and Nanofluids, they have shown the results for industrial uses. When taken as a whole, these investigations provide light on the intricate interactions between magnetic fields, thermal diffusion, and chemical processes in fluid systems, providing useful answers to problems in engineering and industry. Every one of the above examples demonstrates how fluid flows are important in heat and mass transfer and highlights the importance of both understanding and optimizing the processes at work.

Examining the nanofluid is the driving force behind this project domain that is affected by thermophoresis, Brownian motion, magnetic fields, and Casson fluid particles on an exponentially expanding surface in three-dimensional orientations. This work is based on earlier research that has been published. To study how the time, it takes for heat to relax affects the temperature of the fluid, the thickness of the boundary layer, and the heat transfer coefficient, the Cattaneo Christov heat flow effects are employed. While we were looking at the model, we made a list of all of its physical qualities. This was done before we looked at the physical properties of the problem. We made use of governing equations and essential principles to build the issue, which incorporates the Cattaneo-Christov heat flow as well as the magnetohydrodynamic effects. The model's fundamental partial differential equations are extremely nonlinear and have been changed into a form that is not dimensional by the use of similarity transformations. The Runge Kutta method along with the shooting approach was used to achieve numerical resolution of the non-dimensional system of equations that was produced as a consequence. We have conducted a visual exploration of the impact that a variety of dimensionless components have on the flow field by making use of graphical representations. For these physical parameters, for example, thus, we have quantitatively estimated and presented the Nusselt number and skin friction factor.

2 Flow Governing Equations

In this paper, we investigate the three-dimensional flow behavior of an incompressible, viscous, and electrically charged Casson-Nanofluid. The present investigation incorporates Brownian motion, thermophoresis, nanofluid particles, a magnetic field, and porous media. A thorough examination of the interplay between these factors is conducted to elucidate their cumulative impact on the fluid flow characteristics. The physical configuration of the fluid flow for this inquiry is shown in Fig. 1. Following established methodologies, the following key assumptions have been made to ensure the validity and reliability of the research findings. These assumptions are based on a thorough review of the existing literature and are deemed essential for the successful execution of this study.

(a) Thermal relaxation time effect is considered in an energy equation.

(b) Let us consider a system that is exposed to a homogeneous transverse magnetic field parallel to the z-axis and with strength of Bo.

(c) The Magnetic Reynolds number is frequently deemed sufficiently diminutive. Consequently, this justifies the omission of induced magnetic and electric fields from our analytical considerations. This assumption is pivotal in simplifying the complex interactions within the fluid, allowing for a more tractable examination of the magnetic field's behavior under such conditions.

(d) The convective boundary condition involves heating the sheet surface with an evenly heated fluid (Tf) and a convective transfer of heat coefficient (hf) are all necessary components.

(e) Thermal radiation, the energy equation ignores Dufour, joule heating and viscous dissipation.

(f) The boundary conditions neglect the multiple slip effects.

(g) A magnetic field effect is included in the two momentum equations.

(h) The values of energy and concentration are calculated with regard to the influence of thermophoresis and Brownian motion, where appropriate.

(i) It is assumed that Soret and chemical reaction impacts are excluded in the concentration formula and thus cannot be included in the analysis of the process.

(j) The effect of massive relaxation time is considered in the concentration equation.

(k) The border conditions account for the influence of the convective boundary condition.

(l) A non-Newtonian fluid's rheological equation is as follows:

$$\tau = \tau_o + \mu\alpha^* \tag{1}$$

Eq. (1) can be expanded for Casson fluid as:

$$\tau_{ij} = \begin{cases} 2\left(\mu_B + \dfrac{p_y}{\sqrt{2\pi}}\right) e_{ij}, & \pi > \pi_c \\ 2\left(\mu_B + \dfrac{p_y}{\sqrt{2\pi_c}}\right) e_{ij}, & \pi < \pi_c \end{cases} \tag{2}$$

where $\pi = e_{ij}e_{ji}$ with e_{ij}.

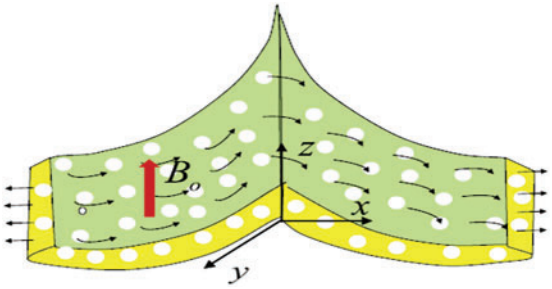

Figure 1: Physical representation of Casson-Nanofluid flow

In the realm of scientific inquiry, these equations serve as the cornerstone, providing a framework for understanding and predicting the behavior of systems under investigation. The intricate interplay between mass, momentum, energy, and nanoparticle concentration is encapsulated within these equations, offering valuable insights into the complex dynamics that govern such systems. In the context of the aforementioned premises, the fundamental equations governing mass conservation are as follows:

Continuity equation:

$$\frac{\partial u}{\partial x} + \frac{\partial v}{\partial y} + \frac{\partial w}{\partial z} = 0 \tag{3}$$

Momentum equation:

$$u\left(\frac{\partial u}{\partial x}\right) + v\left(\frac{\partial u}{\partial y}\right) + w\left(\frac{\partial u}{\partial z}\right) = \nu_f\left(1 + \frac{1}{\beta}\right)\left(\frac{\partial^2 u}{\partial z^2}\right) - \left(\frac{\nu_f}{K^*}\right)u - \left(\frac{\sigma B_o^2}{\rho_f}\right)u \tag{4}$$

$$u\left(\frac{\partial v}{\partial x}\right) + v\left(\frac{\partial v}{\partial y}\right) + w\left(\frac{\partial v}{\partial z}\right) = \nu_f\left(1 + \frac{1}{\beta}\right)\left(\frac{\partial^2 v}{\partial z^2}\right) - \left(\frac{\nu_f}{K^*}\right)v - \left(\frac{\sigma B_o^2}{\rho_f}\right)v \tag{5}$$

Equation of thermal energy:

$$u\left(\frac{\partial T}{\partial x}\right)+v\left(\frac{\partial T}{\partial y}\right)+w\left(\frac{\partial T}{\partial z}\right)=\alpha_f\left(\frac{\partial^2 T}{\partial z^2}\right)+\tau_B\left\{D_B\left(\frac{\partial T}{\partial z}\right)\left(\frac{\partial C}{\partial z}\right)+\frac{D_T}{T_\infty}\left(\frac{\partial T}{\partial z}\right)^2\right\}$$
$$-\omega_1\begin{pmatrix}u^2\frac{\partial^2 T}{\partial x^2}+v^2\frac{\partial^2 T}{\partial y^2}+w^2\frac{\partial^2 T}{\partial z^2}+\left(u\frac{\partial u}{\partial x}+v\frac{\partial u}{\partial y}+w\frac{\partial u}{\partial z}\right)\frac{\partial T}{\partial x}\\ \left(u\frac{\partial v}{\partial x}+v\frac{\partial v}{\partial y}+w\frac{\partial v}{\partial z}\right)\frac{\partial T}{\partial y}+\left(u\frac{\partial w}{\partial x}+v\frac{\partial w}{\partial y}+w\frac{\partial w}{\partial z}\right)\frac{\partial T}{\partial z}\\ +2uv\frac{\partial^2 T}{\partial x\partial y}+2vw\frac{\partial^2 T}{\partial y\partial z}+2uw\frac{\partial^2 T}{\partial x\partial z}\end{pmatrix} \tag{6}$$

Equation of species concentration:

$$u\left(\frac{\partial C}{\partial x}\right)+v\left(\frac{\partial C}{\partial y}\right)+w\left(\frac{\partial C}{\partial z}\right)=D_B\left(\frac{\partial^2 C}{\partial z^2}\right)+\frac{D_T}{T_\infty}\left(\frac{\partial T}{\partial z}\right)^2$$
$$-\omega_2\begin{pmatrix}u^2\frac{\partial^2 C}{\partial x^2}+v^2\frac{\partial^2 C}{\partial y^2}+w^2\frac{\partial^2 C}{\partial z^2}+\left(u\frac{\partial u}{\partial x}+v\frac{\partial u}{\partial y}+w\frac{\partial u}{\partial z}\right)\frac{\partial C}{\partial x}\\ \left(u\frac{\partial v}{\partial x}+v\frac{\partial v}{\partial y}+w\frac{\partial v}{\partial z}\right)\frac{\partial C}{\partial y}+\left(u\frac{\partial w}{\partial x}+v\frac{\partial w}{\partial y}+w\frac{\partial w}{\partial z}\right)\frac{\partial C}{\partial z}\\ +2uv\frac{\partial^2 C}{\partial x\partial y}+2vw\frac{\partial^2 C}{\partial y\partial z}+2uw\frac{\partial^2 C}{\partial x\partial z}\end{pmatrix} \tag{7}$$

The flow's boundary conditions are:

$$\left.\begin{array}{l}u=U_w=U_o\exp\left(\frac{x+y}{L}\right),\quad v=V_w=V_o\exp\left(\frac{x+y}{L}\right),-\kappa_f\left(\frac{\partial T}{\partial z}\right)=h_f\left(T_f-T\right),\quad C=C_w\ at\ z=0\\ u\to 0,v\to 0,T\to T_\infty,\quad C\to C_\infty as\ z\to\infty\end{array}\right\} \tag{8}$$

Proposed similarity transformations are as follows:

$$\left.\begin{array}{l}u=U_o\exp\left(\frac{x+y}{L}\right)f'(\eta),\ v=V_o\exp\left(\frac{x+y}{L}\right)g'(\eta),\ \theta=\frac{T-T_\infty}{T_f-T_\infty},\ \phi=\frac{C-C_\infty}{C_w-C_\infty},\\ w=-\sqrt{\frac{\nu_f U_o}{2}}\exp\left(\frac{x+y}{2L}\right)\{f(\eta)+\eta f'(\eta)+g(\eta)+\eta g'(\eta)\},\ \eta=\left(\sqrt{\frac{U_o}{2\nu_f L}}\right)\exp\left(\frac{x+y}{2L}\right)z,\end{array}\right\} \tag{9}$$

By Eq. (9), the above (4) to (7) equations are of the below form:

$$\left(1+\frac{1}{\beta}\right)f'''-2f'^2+ff''+gf''-2f'g'-Mf'-Kf'=0 \tag{10}$$

$$\left(1+\frac{1}{\beta}\right)g'''-2g'^2-2f'g'+fg''+gg''-Mg'-Kg'=0 \tag{11}$$

$$\theta''+\Pr f\theta'+\Pr g\theta'+\Pr Nb\theta'\phi'+\Pr Nt\theta'^2-\Pr Nb\omega\left\{(f+g)^2\theta''+(f+g)(f'+g')\theta'\right\}=0 \tag{12}$$

$$Nb\phi''+NbScf\phi'+NbScg\phi'+Nt\theta''-NbSc\delta\left\{(f+g)^2\phi''+(f+g)(f'+g')\phi'\right\}=0 \tag{13}$$

The matching boundary conditions (6) transform into:

$$\left.\begin{array}{l} f(0)=g(0)=0, g'(0)=S, f'(0)=\varphi(0)=1,\ \theta'(0)=-Bi\{1-\theta(0)\} \\ f'(\infty)\to 0, \\ g'(\infty)\to 0, \theta(\infty)\to 0, \varphi(\infty)\to 0 \end{array}\right\} \tag{14}$$

wherein the relevant physical characteristics are described as:

$$\left.\begin{array}{l} M=\dfrac{2\sigma B_o^2 L}{\rho_f U_w},\ K=\dfrac{2\nu_f L}{K^* U_w},\ S=\dfrac{V_o}{U_o},\ \varepsilon=\exp\left(\dfrac{x+y}{L}\right),\ Nb=\dfrac{\tau_B D_B (C_w-C_\infty)}{\nu_f},\ \Pr=\dfrac{\nu_f}{\alpha_f}, \\ Nt=\dfrac{\tau_B D_T (T_f-T_\infty)}{\nu_f T_\infty},\ Sc=\dfrac{\nu_f}{D_B},\ h_f=\dfrac{\varepsilon}{\exp\left(\dfrac{x+y}{2L}\right)},\ Bi=\dfrac{\varepsilon}{\kappa_f}\sqrt{\dfrac{2\nu_f L}{U_o}}, \end{array}\right\} \tag{15}$$

The following are physically significant quantities:

$$Cf_x=\frac{2\tau_{wx}}{\rho_f U_w^2}\Rightarrow Cf_x\left(\sqrt{\frac{\mathrm{Re}_x}{2}}\right)=f''(0) \tag{16}$$

$$Cf_y=\frac{2\tau_{wy}}{\rho_f V_w^2}\Rightarrow\left(\sqrt{\frac{\mathrm{Re}_y}{2}}\right)Cf_y=g''(0) \tag{17}$$

$$Nu_x=\frac{xq_w}{\kappa_f (T_f-T_\infty)}=-\frac{x\left(\dfrac{\partial T}{\partial z}\right)_{z=0}}{\kappa_f (T_f-T_\infty)}\Rightarrow Nu_x=-\frac{x}{L}\left(\sqrt{\frac{\mathrm{Re}_x}{2}}\right)\theta'(0) \tag{18}$$

$$Sh_x=\frac{xq_m}{D_B (C_w-C_\infty)}=-\frac{x\left(\dfrac{\partial C}{\partial z}\right)_{y=0}}{D_B (C_w-C_\infty)}\Rightarrow Sh_x=-\frac{x}{L}\left(\sqrt{\frac{\mathrm{Re}_x}{2}}\right)\phi'(0) \tag{19}$$

3 Methods

Because the governing equations have non-linear partial derivatives, the following practical approach is employed: It has been used the Runge-Kutta method and the shooting technique method to solve the problem. By employing these advanced techniques, experts can navigate complex mathematical problems with precision and accuracy, ultimately leading to valuable insights and discoveries in various fields of study. This approach produces more accurate outcomes when compared to alternative numerical methods. To make partial differential equations easier to handle, similar transformations are employed, ideally to make them ordinary differential equations. This mathematical technique enables the reduction of complex, nonlinear systems to a set of simpler, linear equations, thereby facilitating a more in-depth analysis of the underlying dynamics. Introducing additional variables into a higher-order differential equation to convert it into a linear equation:

$$f_1=f,\ f_2=f',\ f_3=f'',\ f_4=g,\ f_5=g',\ f_6=g'',\ f_7=\theta,\ f_8=\theta',\ f_9=\phi,\ f_{10}=\phi'\} \tag{20}$$

The first order ODE that follows is obtained by transforming Eqs. (13)–(15):

$$\left.\begin{aligned} f_3 = f_2',\ f_3' &= \frac{2f_2^{\,2} - f_1 f_3 - f_4 f_3 + 2f_2 f_5 + Mf_2 + Kf_2}{\left(1+\frac{1}{\beta}\right)} \\ f_6 = f_5',\ f_6' &= \frac{2f_5^{\,2} + 2f_2 f_5 - f_1 f_6 - f_4 f_6 + Mf_5 + Kf_5}{\left(1+\frac{1}{\beta}\right)}, \\ f_8' &= \frac{-\Pr f_1 f_8 - \Pr f_4 f_8 - \Pr Nbf_8 f_{10} - \Pr Ntf_8^{\,2} + \Pr Nb\omega\,(f_1+f_4)\,(f_2+f_5)\,f_8}{\left[1-\Pr Nb\omega\,(f_1+f_4)^2\right]}, \\ f_{10}' &= \frac{-NbScf_1 f_8 - NbScf_4 f_{10} - Ntf_8' + NbSc\delta\,(f_1+f_4)\,(f_2+f_5)\,f_{10}}{Nb\left[1-Nb\delta\,(f_1+f_4)^2\right]} \end{aligned}\right\} \tag{21}$$

The matching boundary conditions (14) are determined by using Eq. (20).

$$\left.\begin{aligned} &f_1(0)=0, f_4(0)=0, f_2(0)=1, f_5(0)=S,\ f_7(0)=-Bi\{1-f_7(0)\},\ f_9(0)=1 \\ &f_2(\infty)\to 0, f_5(\infty)\to 0, f_7(\infty)\to 0, f_9(\infty)\to 0 \end{aligned}\right\} \tag{22}$$

Graphical representations of approximate solutions were generated to demonstrate the physical implications of non-dimensional parameters, and a MATLAB bvp4c solver was applied. An iteration technique was used where the iteration was continued until a prespecified level of precision of 10^{-6} was attained.

Program Code Validation

In order to evaluate the computer code, the results that were produced are compared and validated with the existing literature, as shown by Nayak et al. [45] in Table 1. However, the influences of Casson fluid and Cattaneo-Christov double diffusion are not taken into consideration. Using this comparison and validation approach, we can ensure that our numerical findings exhibit a high degree of consistency, which in turn highlights the correctness of our results.

Table 1: Validation of present skin-friction coefficient along x and y-directions results

M	Skin-friction results along x	Results of [45]	Skin friction results along y	Results of [45]
0.0	1.15527530273	1.163721	2.5385827105	2.587412
10.0	3.3560672320	3.377240	4.3581576015	4.378350
100.0	10.0025630238	10.076473	12.0458502732	12.076473

4 Results and Discussion

Using the same boundary conditions, the present mathematical model includes the Casson-Nanofluid to investigate the impacts of Cattaneo-Christov double diffusion, convective boundary conditions, magnetic fields, Brownian motion, porous media, and thermophoresis. Three main nonlinear partial differential equations (PDEs) form this physics problem. The equations include concentration, energy, and motion. A collection of partial and non-linear ordinary differential equations (ODEs) is generated with similarity transformations. They are solved using the R-K technique in concert with the

shooting approach to get precise answers considering the boundary conditions. We investigate many factors and evaluate how they affect the results. One looks at these parts using tables and graphs. The results of the study may be viewed in Table 1. Through Figs. 2 and 3, the changes of the magnetic field parameter concerning the main profile and the velocity profile are presented, respectively. An analogous resistive force to drag, the Lorentz force develops as M increases in magnitude. The Lorentz force stops motion and stops velocity profiles. Figs. 4 and 5, respectively, show how the permeability parameter affects the primary and secondary velocity patterns. Numerical results show an inverse relationship between velocity profiles and porosity parameter K, a higher value for K results in a lower velocity profile. This is because, as K increases, the momentum barrier layer becomes thinner due to the simultaneous growth of the porous layer. Figs. 6 and 7 show how the primary and secondary velocity patterns are affected.

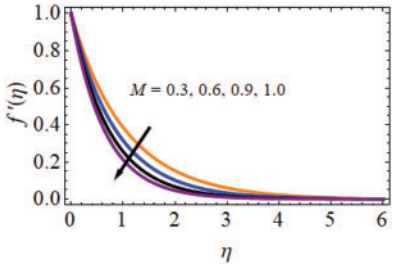

Figure 2: Primary velocity profiles: M effect

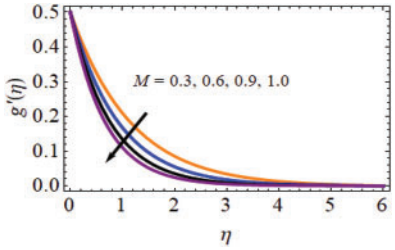

Figure 3: M effect: secondary velocity profiles

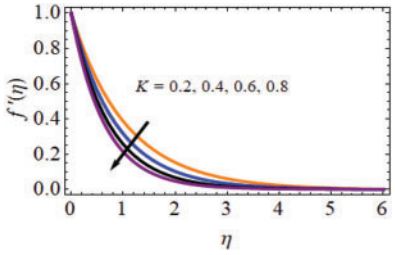

Figure 4: K effect on primary velocity profiles

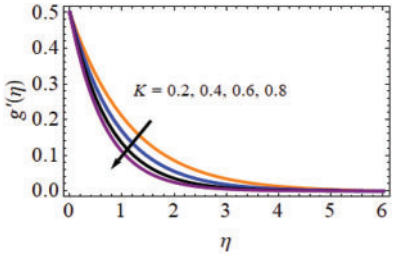

Figure 5: Secondary velocity profiles: K effect

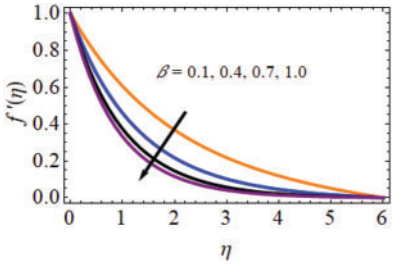

Figure 6: Primary velocity profiles: effect of β

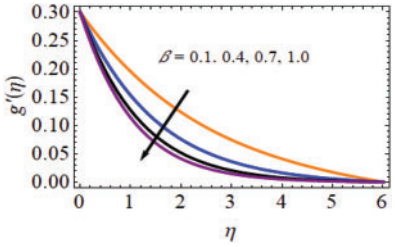

Figure 7: Secondary velocity profiles: effect of β

Fig. 8, as a function of the Prandtl number, shows how the distribution of temperatures changes. A higher Prandtl number is associated with a lower temperature field value and a thinner thermal layer. When the thermal diffusivity drops with increasing Prandtl number, a weaker temperature field and a smaller thermal layer are produced. Figs. 9 and 10 show how Nb affects the temperature and concentration curves; in Fig. 9, low Nb can perhaps improve the temperature profiles. Fig. 9 shows these three processes, thermal boundary layer formation, and temperature increase. This rise is attributed in part to a higher Brownian motion parameter, lower viscous force, and stronger Brownian diffusion coefficient. Fig. 10 shows that concentration decreases concomitantly with increasing *Nb*. Figs. 11 and 12 correspondingly contributes to the investigation of examination of the impact of the thermophoresis parameter (Nt) on temperature and concentration profiles. Viewable below are the following profiles. The heat diffusion coefficient and the viscous force are used to calculate the thermophoresis parameter accurately. Given that viscous force and the thermophoresis parameter Nt are inversely correlated, increasing Nt leads to a decrease in viscous force while concurrently increasing the heat diffusion coefficient. This phenomenon causes higher temperature values and higher nanoparticle density. The influence of the thermal relaxation time parameter is investigated in Fig. 13 for the temperature distribution analysis. This result can be analyzed as if the Thermal

Relaxation Time Parameter (ω) increases the temperature profiles decrease. The influence of the mass relaxation time parameter (δ) on the temperature distributions can be inferred from Fig. 14. The concentration profiles of the element are less sensitive when the parameter of mass relaxation time is increased. It can also be seen from Fig. 15 that the thermal Biot number (Bi) has a straight proportional with temperature distributions. The problem of the Thermal Biot number is referred to in the analysis of the convection coefficient. Bi = 0 the results confirm the nonexistence of heat transfer through the wall. With a higher Thermal Biot number (Bi > 0) the heat transfer rate has altered, and the temperature distribution is higher. Temperature gradient in combination with mass transfer is capable of transferring mass from a region with the least solute concentration to a region with the highest solute concentration. Changes in the concentration distribution with the Schmidt number (Sc) are presented in Fig. 16. Sc is the mass diffusivity to momentum diffusivity ratio where $Sc = \nu/\mathrm{Dm}$. Determination of the relative momentum transfer and the mass by exploring the diffusion inside the species' concentration boundary layer is possible. As the Sc number increases it will lower the mass diffusivity of the fluid and thus lower the variance of the profiles of concentration. Mass diffusivity and the Schmidt number (Sc) show an inverse connection wherein higher Schmidt number values match fewer concentration boundary layers. This results from the interplay of mass diffusivity with Sc.

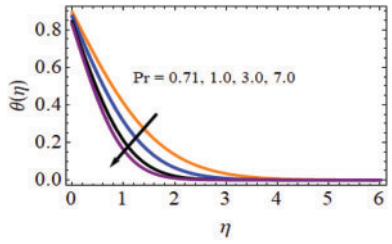

Figure 8: Pr effect: temperature profiles

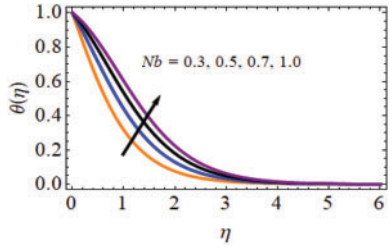

Figure 9: Temperature profiles: effect of Nb

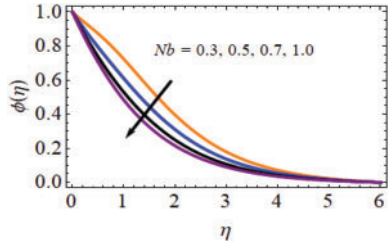

Figure 10: Concentration profiles: effect of Nb

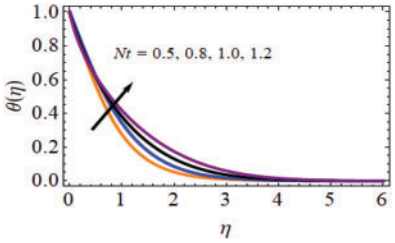

Figure 11: Temperature profiles: effect of *Nt*

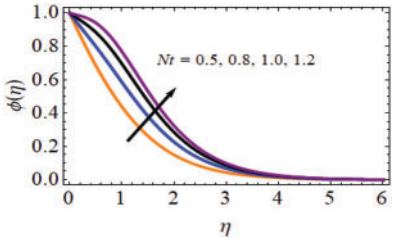

Figure 12: *Nt* effect: concentration profiles

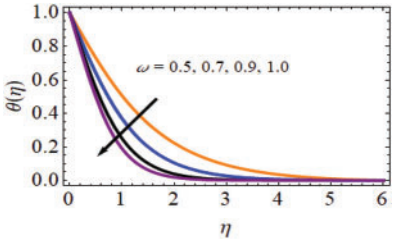

Figure 13: ω effect: temperature profiles

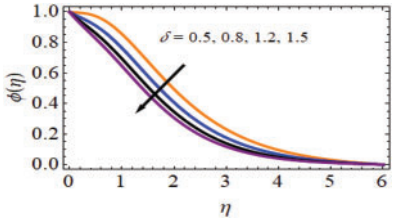

Figure 14: δ effect on concentration profiles

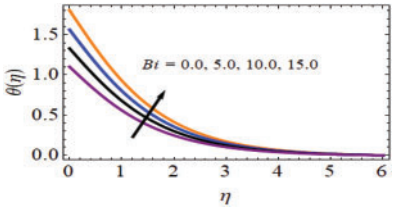

Figure 15: *Bi* effect on temperature profiles

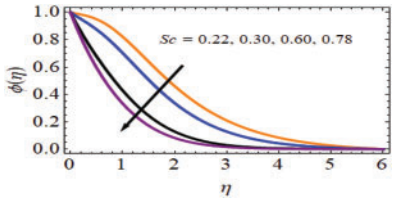

Figure 16: *Sc* effect on concentration profiles

Tables 2 and 3 show the correlation between skin-friction coefficients in x and y directions and various parameters. A positive correlation is found with Thermophoresis, Brownian motion, stretching ratio, and Biot number, while a decrease is observed with increasing values of mass relaxation time, permeability, Casson fluid, Prandtl number, thermal relaxation time, and Schmidt number. Table 4 shows how to facilitate providing numerical values of a heat transfer coefficient that embraces a wide variety of Biot numbers (Bi), Prandtl numbers (Pr), Brownian motion parameters (Nb), thermal relaxation time parameters ($\ddot{\upsilon}$), and Thermophoresis parameters (Nt), the Nusselt number was used. With the increase in Biot number (Bi), It is also found that with the increase in thermophoresis parameter (Nt) and Brownian motion parameter (Nb) the heat transfer coefficient will increase. However, when Pr and $\ddot{\upsilon}$ are large in magnitude, the opposite effect is obtained.

Table 2: Skin-friction coefficient values calculated against velocity profiles

M	K	β	S	Pr	Nt	Nb	ω	Bi	Sc	δ	Cf_x
0.3	0.2	0.1	0.5	0.71	0.5	0.3	0.5	5.0	0.22	0.5	3.6786691355
0.6											3.6480707627
0.9											3.6206671095
	0.4										3.6520721408
	0.6										3.6301856204
		0.4									3.6399580285
		0.7									3.6158928423
			1.0								3.7015708276
			1.5								3.7256062955
				1.00							3.6419952925
				3.00							3.6109872592
					0.8						3.6935087287
					1.0						3.7141438718
						0.5					3.6845629875
						0.7					3.7001598962
							0.7				3.6510756075
							0.9				3.6307652756
								10.0			3.7058287523
								15.0			3.7217658712
									0.30		3.6399875628
									0.78		3.6156812673

(Continued)

Table 2 (continued)

M	K	β	S	Pr	Nt	Nb	ω	Bi	Sc	δ	Cf_x
										0.8	3.6500585286
										1.2	3.6316542694

Table 3: Skin-friction coefficient numerical values resulting from secondary velocity patterns

M	K	β	S	Pr	Nt	Nb	ω	Bi	Sc	δ	Cf_y
0.3	0.2	0.1	0.5	0.71	0.5	0.3	0.5	5.0	0.22	0.5	2.3865760271
0.6											2.3507458762
0.9											2.3356628781
	0.4										2.3697607523
	0.6										2.3490697981
		0.4									2.3606961509
		0.7									2.3408560722
			1.0								2.4165750876
			1.5								2.4408237602
				1.00							2.3565608572
				3.00							2.3345366648
					0.8						2.4260686816
					1.0						2.4456701605
						0.5					2.4006650161
						0.7					2.4261006526
							0.7				2.3626456903
							0.9				2.3454892582
								10.0			2.4156019592
								15.0			2.4325676128
									0.30		2.3557608156
									0.78		2.3264501525
										0.8	2.3695661765
										1.2	2.3410656250

As shown in Table 5, mass transfer coefficient densities for different values of Nb, Nt, Sc, and δ about the parameters of Brownian motion, thermophoresis, mass relaxation time, and Schmidt number. The mass transfer coefficient is a parameter of Brownian motion, and the mass relaxation time parameter affects the heat transfer coefficient negatively, but the thermophoresis parameter enhances the heat transfer coefficient.

Table 4: The heat transfer coefficient's numerical values resulting from temperature profiles

Pr	Nt	Nb	ω	Bi	Nu_x
0.71	0.5	0.3	0.5	5.0	1.8969046523
1.00					1.8523545085
3.00					1.8376851483
	0.8				1.9358072534
	1.0				1.9568687623
		0.5			1.9109768762
		0.7			1.9397687023
			0.7		1.8646576807
			0.9		1.8467075792
				10.0	1.9265067664
				15.0	1.9476009626

Table 5: The mass transfer coefficient's numerical values obtained from concentration profiles

Nt	Nb	Sc	δ	Sh_x
0.5	0.3	0.22	0.5	2.5670625209
0.8				2.6059263692
1.0				2.6359692515
	0.5			2.5966529081
	0.7			2.6265902523
		0.30		2.5209686253
		0.78		2.4912342325
			0.8	2.5378681854
			1.2	2.5140746732

5 Conclusions

In our recent research endeavor, we have meticulously tackled the analytical challenge of numerically resolving the linear differential equations that govern the magneto-hydrodynamic Casson-Nanofluid flow over a stretching sheet. By employing advanced mathematical techniques and leveraging the expertise of our team, we have successfully navigated the complexities of this intricate problem, ultimately contributing to the broader understanding of fluid dynamics in the context of nanofluids and magnetic fields. The results of a magnetic field, thermophoresis, porous substrate, Brownian motion, and Cattaneo Christov double diffusion are considered within this investigation. We study the x- and y-dimensional velocity components, temperature and concentration profiles, the Runge-Kutta method, and shooting approach, as a function of various parameters. Particularly, we examine the effects of different values on the key parameters. This study yielded the following conclusions:

- The primary and secondary velocity patterns decrease as the Casson fluid, permeability, and magnetic field parameters rise.

- The concentration profiles diminish as the Schmidt number, with increasing mass relaxation time and Brownian motion parameters, the trend moves in the opposite direction when the thermophoresis parameter increases.
- The results derived from the present methodology are outstanding and consistent with the conclusions in the absence of Casson fluid and double Cattaneo-Christov diffusion effects.

Acknowledgement: We are thankful to our family members and friends for their kind support.

Funding Statement: The authors received no specific funding for this study.

Author Contributions: The authors confirm contribution to the paper as follows: Study conception and design: Murali Gundagani; Data collection: Venkata Madhu Javvaji; Analysis and interpretation of results: All the authors; Draft manuscript preparation: All the authors. All authors reviewed the results and approved the final version of the manuscript.

Availability of Data and Materials: The datasets used and/or analysed during the current study are available from the corresponding author on reasonable request and all data generated or analyzed during this study are included in this published article.

Ethics Approval: Not applicable.

Conflicts of Interest: The authors declare no conflicts of interest to report regarding the present study.

References

1. Nadeem S, Lee C. Series solution of magneto-hydrodynamic boundary layer flow over bi-directional exponentially stretching surfaces. J Braz Soc Mech Sci Eng. 2016;38(2):443–53. doi:10.1007/s40430-015-0344-2.
2. Akbar N, Khan Z, Nadeem S, Khan W. Double-diffusive natural convective boundary-layer flow of a nanofluid over a stretching sheet with magnetic field. Int J Numer Methods Heat Fluid Flow. 2016;26(1): 108–21. doi:10.1108/HFF-01-2015-0019.
3. Sadiq MA, Nadeem S. Unsteady MHD boundary layer flow of a couple stress nano fluid over a stretching/shrinking surface with convective boundary condition. J Comput Theor Nanosci. 2015;12(11):4408–14. doi:10.1166/jctn.2015.4376.
4. Ali A, Khan MDN, Ali A. Analysis of flow and heat transfer over stretching/shrinking and porous surfaces. J Plast Film Sheeting. 2022;38(1):21–45. doi:10.1177/87560879211025805.
5. Hussain S, Rasheed K, Ali A, Vrinceanu N, Alshehri A, Shah Z. A sensitivity analysis of MHD nanofluid flow across an exponentially stretched surface with non-uniform heat flux by response surface methodology. Sci Rep. 2022;12(1):18523. doi:10.1038/s41598-022-22970-y.
6. Hsiao KL. Stagnation electrical MHD nanofluid mixed convection with slip boundary on a stretching sheet. Appl Therm Eng. 2016;98:850–86. doi:10.1016/j.applthermaleng.2015.12.138.
7. Awais M, Hayat T, Ali A, Irum S. Velocity, thermal and concentration slip effects on a magneto-hydrodynamic nanofluid flow. Alex Eng J. 2016;55(3):2107–14. doi:10.1016/j.aej.2016.06.027.
8. Khashiie NS, Arifin NM, Pop I, Nazar R, Hafidzuddin EH, Wahi N. Three-dimensional hybrid nanofluid flow and heat transfer past a permeable stretching/shrinking sheet with velocity slip and convective condition. Chin J Phys. 2020;66(4):157–71. doi:10.1016/j.cjph.2020.03.032.
9. Makinde OD, Aziz A. Boundary layer flow of a nanofluid past a stretching sheet with a convective boundary condition. Int J Therm Sci. 2011;50(7):1326–32. doi:10.1016/j.ijthermalsci.2011.02.019.

10. Khan WA, Pop I. Boundary-layer flow of a nanofluid past a stretching sheet. Int J Heat Mass Transf. 2010;53:2477–83. doi:10.1016/j.ijheatmasstransfer.2010.01.032.
11. Cattaneo C. Sulla conduzione del calore. Atti Semin Mat Fis Univ Modena. 1948;3:83–101.
12. Mustafa M. Cattaneo-Christov heat flux model for rotating flow and heat transfer of upper-convected Maxwell fluid. AIP Adv. 2015;5(4):47109. doi:10.1063/1.4917306.
13. Ciarletta M, Straughan B. Uniqueness and structural stability for the Cattaneo-Christov equations. Mech Res Commun. 2010;37(5):445–7. doi:10.1016/j.mechrescom.2010.06.002.
14. Straughan B. Thermal convection with the Cattaneo-Christov model. Int J Heat Mass Transf. 2010;53(1):95–8. doi:10.1016/j.ijheatmasstransfer.2009.10.001.
15. Han S, Zheng L, Li C, Zhang X. Coupled flow and heat transfer in viscoelastic fluid with Cattaneo-Christov heat flux model. Appl Math Lett. 2014;38:87–93. doi:10.1016/j.aml.2014.07.013.
16. Babu NVN, Murali G, Bhati SM. Casson fluid performance on natural convective dissipative couette flow past an infinite vertically inclined plate filled in porous medium with heat transfer, MHD and hall current effects. Int J Pharm Res. 2018;10(4):809–19.
17. Deepa G, Murali G. Effects of viscous dissipation on unsteady MHD free convective flow with thermophoresis past a radiate inclined permeable plate. Iran J Sci Technol Trans. 2014;38(A3):379–88.
18. Kirubaharan DR, Subhashini AD, Murali G. Study of three dimensional casson-nanofluid flow due to a linear porous stretching sheet in the presence of double diffusion effects. Adv Syst Sci Appl. 2024;24(3):90–103. doi:10.25728/assa.2024.2024.03.1539.
19. Gundagani M, Babu NVN, Gadially D, Bhati SM, Sanjay CH, Nirmala KV. Study of nano-powell-erying fluid flow past a porous stretching sheet by the effects of mhd, thermal and mass convective boundary conditions. J Umm Al-Qura Univ Eng Archit. 2024;15(3):271–81. doi:10.1007/s43995-024-00056-2.
20. Gundagani M, Mamidi LP, Tanuku PK. Finite element solutions of double diffusion effects on three-dimensional MHD Nano-Powell-Erying fluid flow in presence of thermal and mass Biot numbers. J Eng Appl Sci. 2024;71(1):9. doi:10.1186/s44147-023-00347-w.
21. Murali G, Deepa G, Madhu JV, Kasturi VN, Bhati SM, Babu NN. Three dimensional chemically reacting oldroyd-b fluid + nanofluid flow in presence of thermophoresis and brownian motion effects. Discontinuity Nonlinearity Complex. 2025;14(2):373–88. doi:10.5890/DNC.2025.06.010.
22. Murali G, Deepa G, Nirmala Kasturi V, Poornakantha T. Joint effects of thermal diffusion and diffusion thermo on MHD three dimensional nanofluid flow towards a stretching sheet. Math Models Eng. 2023;9(4):130–43. doi:10.21595/mme.2023.23590.
23. Murali G, Babu NVN. Convective MHD jeffrey fluid flow due to vertical plates with pulsed fluid suction: a numerical Study. J Comput Appl Mech. 2023;54(1):36–48.
24. Bhati SM, Murali G, Sanjay CH. Law of elecric fields via bianchi identities. J Appl Sci Eng. 2022;25(4):759–62. doi:10.6180/jase.202208_25(4).0011.
25. Nagasmitha BR, Nagendramma V, Ahmed N, Marutamanikandan S, Murali G. Mathematical modeling of heat transfer phenomena in darcy porous media with couple-stress magnetic fluid under maxwell-cattaneo model. J Mines Met Fuels. 2025;73(2):509–16. doi:10.18311/jmmf/2025/47825.
26. Tanuku PK, Mamidi LP, Gundagani M. Modelling and analysis of three-dimensional chemically reacting, radiating Casson-nanofluid flow: thermophoresis and Brownian motion effects. Acta Polytech. 2024;64(5):455–63. doi:10.14311/AP.2024.64.0455.
27. Sivaiah S, Gundagani M, Karanamu MP. Analysis of heat and mass transfer effects on an isothermal vertical oscillating plate. Walailak J Sci Technol. 2012;9(4):407–15.
28. Nagasmitha BR, Nagendramma V, Ahmed N, Marutamanikandan S, Murali G. Analytical study of nonlinear behavior and convection patterns in darcy-brinkman porous medium with maxwell-cattaneo ferroconvection. J Mines Met Fuels. 2025;73(2):437–45. doi:10.18311/jmmf/2025/47828.

29. Gundagani M, Sheri S, Paul A, Reddy MCK. Radiation effects on an unsteady MHD convective flow past a semi-infinite vertical permeable moving plate embedded in a porous medium with viscous dissipation. Walailak J Sci Technol. 2013;10(5):499–515. doi:10.2004/wjst.v10i5.380.
30. Poornakantha T, Laksmiprsanna M, Murali G. Modelling and analysis of three-dimensional maxwell-nanofluid flow over a bi-directional stretching surface in the presence of a magnetic field. Int J Eng Model. 2025;38(1):53–72. doi:10.31534/engmod.2025.1.ri.04d.
31. Madan KR, Srinivasa RR, Kumar MA, Venkateswarlu B. A numerical study of thermal and diffusion effects on MHD Jeffrey fluid flow over a porous stretching sheet with activation energy. Numer Heat Transf Part A Appl. 2024;11(3):1–22. doi:10.1080/10407782.2024.2319344.
32. Venkatesh N, Raju RS, Anil Kumar M, Dharmendar RY. A numerical study on MHD Maxwell fluid with nanoparticles over a stretching surface: impacts of thermal radiation, convective boundary condition and induced magnetic field. Numer Heat Transf Part A Appl. 2024:1–16. doi:10.1080/10407782.2024.2338259.
33. Rajakumar KVB, Ranganath N, Govinda RT, Srinivasa RR. Radiation absorption, Hall and ion-slip current—driven MHD convection with spanwise cosinusoidally fluctuating temperature: a perturbative study. Radiat Eff Defects Solids. 2024;43(1):1–35. doi:10.1080/10420150.2024.2391775.
34. Suhasini R, Srinivasa RR, Anil KM, Dharmendar RY, Madan KR. A numerical study on MHD micropolar nanofluid flow over a Darcian porous stretching surface: impacts of thermophoretic and Brownian diffusions. Radiat Eff Defects Solids. 2024;179(11–12):1616–31. doi:10.1080/10420150.2024.2359679.
35. Mebarek-Oudina F, Dharmaiah G, Balamurugan KS, Ismail AI, Saxena H. The role of quadratic-linearly radiating heat source with carreau nanofluid and exponential space-dependent past a cone and a wedge: a medical engineering application and renewable energy. J Comput Biophys Chem. 2023;22(8):997–1011. doi:10.1142/S2737416523420073.
36. Anantha Kumar DK. A computational model for the density of motile micro-organisms in the Casson fluid flow with thermal radition. J Nav Archit Mar Eng. 2024;21(1):79–86. doi:10.3329/jname.v21i1.70396.
37. Anantha KK, Sugunamma V, Sandeep N. Influence of variable viscosity on 3-D MHD radiative cross nanofluid flow over a biface region. Waves Random Complex Media. 2022;56(2):1–16. doi:10.1080/17455030.2022.2104953.
38. Rathore N, Kumar KA, Sandeep N. Analysis of nanomodels for nanofluid flow over a curved region with MXene (Ti_3C_2). J Therm Anal Calorim. 2024;1–8. doi:10.1007/s10973-024-13916-9.
39. Elattar S, Khan U, Zaib A, Ishak A, Saleh W, Abed AM. Scrutinization of waste discharge concentrations in eyring-powell nanofluid past a deformable horizontal plane surface. Water. 2023;15(19):3419. doi:10.3390/w15193419.
40. Khan U, Zaib A, Ishak A, MSherif ES, Sarris IE. Numerical analysis of irregular heat source/sink through a wall jet flow of spherical graphene oxide nanoparticle in the presence of thermophoretic particle deposition: the case of non-Newtonian Eyring—Powell fluid model. Numer Heat Transf Part B Fundam. 2023;86(1):1–18. doi:10.1080/10407790.2023.2275726.
41. Dharmaiah G, Mebarek-Oudina F, Prasad JR, Rani CB. Exploration of bio-convection for slippery two-phase Maxwell Nanofluid past a vertical induced magnetic stretching regime associated for biotechnology and engineering. J Mol Liq. 2023;391(1):123408. doi:10.1016/j.molliq.2023.123408.
42. Ramesh K, Mebarek-Oudina F, Souayeh B. Mathematical modelling of fluid dynamics and nanofluids. Boca Raton, FL, USA: CRC Press; 2023. doi:10.1201/9781003299608.
43. Raza J, Mebarek-Oudina F, Ali H, Sarris IE. Slip effects on casson nanofluid over a stretching sheet with activation energy: RSM analysis. Front Heat Mass Transf. 2024;22(4):1017–41. doi:10.32604/fhmt.2024.052749.

44. Mezaache A, Mebarek-Oudina F, Vaidya H, Ramesh K. Impact of nanofluids and porous structures on the thermal efficiency of wavy channel heat exchanger. Int J Therm Sci. 2025;210(6):109673. doi:10.1016/j.ijthermalsci.2024.109673.
45. Nayak MK, Akbar NS, Tripathi D, Pandey VS. Three dimensional MHD flow of nanofluid over an exponential porous stretching sheet with convective boundary conditions. Therm Sci Eng Prog. 2017;3: 133–40.